13th International Symposium on Particle Image Velocimetry – ISPIV 2019
Munich, Germany, July 22-24, 2019

Geometric Scattering Removal in CC-DGV by Structured Illumination

Matthew Boyda[1]*, Gwibo Byun[1], Ashley Saltzman[1], K. Todd Lowe[1]

[1]Virginia Tech, Kevin T. Crofton Dept. of Aerospace and Ocean Engineering, Blacksburg VA, USA

*Corresponding Author: boyda13@vt.edu

Abstract

The application of structured illumination for background removal is presented in the current work as a simple imaging technique to significantly reduce the biases introduced into planar, Doppler-based velocimetry measurements by recording the background and signal intensity profiles simultaneously. To the authors' knowledge, this is the first demonstration of structured illumination background removal in this type of measurement. Specifically, in the current work we look at the application of this technique in cross-correlation Doppler global velocimetry (CC-DGV) to remove background contributions in a turbulent free jet with an exit Mach number of 0.5 and high intensity background scattering via the nozzle used and its proximity to a curved wall boundary. Measurements with structured illumination background subtraction are compared with pressure probe measurements. The root-mean-square (RMS) difference between the CC-DGV using the structured illumination method and probe measurements are shown to be 1.2 m/s, well within the published uncertainty bound of this velocity evaluation technique.

1 Introduction

Many applications in aeronautics research currently benefit from the robust and minimally intrusive optical measurements available today due to continuously advancing laser-based technologies. This is particularly true for in situ measurements of complex aerodynamic systems. For example, Virginia Tech has previously applied three-component particle image velocimetry (PIV) to study the complex vortical flows like those seen in advanced propulsion/airframe integration concepts [Nelson et al. (2014), Guimarães et al. (2016) and Guimarães et al. (2017)]. In addition to the application of PIV, other optical diagnostics, such as cross-correlation Doppler global velocimetry (CC-DGV) for three-component velocity [Cadel et al. (2015) and Boyda et al. (2018)], and filtered Rayleigh scattering (FRS), for multi-property measurements [Yeaton et al. (2012), Doll et al. (2014), Doll et al. (2018), and Boyda et al. (2019)], are being developed and applied for these same types of in situ measurements. The reason these techniques are gaining traction for measurements in these conditions is that in comparison to the intrusive conventional probe measurements most often used (e.g., Pitot-static, Kiel, 5-hole probes, and probe rakes), optical diagnostics provide flow information while minimally impacting the flow being studied and, as a major added benefit, providing this information at much higher spatial resolutions.

When any diagnostic technique (probes, optical, etc.) is applied for complicated in-situ measurements, there are always added difficulties with measuring flow conditions near physical hardware boundaries. Near these boundaries, whether a duct/tunnel wall or a model placed in a wind tunnel, is often where the most interesting regions of the flow for study are located. For the case of diagnosing turbomachinery inlet flows as discussed previously, measurements near duct walls provide the greatest challenge. For instance, when using probes, measuring conditions near physical boundaries causes increased flow interaction via the probe-plate potential flow solution, leading to inaccurate measurements [Treaster and Yocum (1978)]. The story is not completely better for applications of optical techniques: the laser light used to measure the flow typically scatters intensely

off the physical surfaces and reduces or eliminates the possibility to measure the desired flow properties accurately due to the domination of scattered light off the duct walls. This geometrically scattered light carries no flow information and obscures the desired signal from the tracer particles in the flow.

The most common means to avoid the effects of background scattering in most laser-based velocity measurements (e.g. PIV, DGV, and FRS) is to position cameras in such a way that either the geometric scattering is not seen or is being viewed at a grazing angle which reduces the effective intensity. The downside to this method is that it can only be used in facilities that can successfully accommodate these viewing configurations, and in most in situ hardware applications this arrangement is not possible: alternative methods must be used. In conventional DGV and PIV applications, background images can be taken without seed in the flow in order to subtract the background intensity from signal images. This method is generally effective but does not remove the secondary scattering caused by light reflecting off particles now present in the flow to geometrical surfaces. Frequency scanning DGV methods such as CC-DGV present another complication in that background images must be taken at every laser frequency used in the scan. Not only does this add measurement time, it adds uncertainty in the measurement if the background images are not taken at the exact same set of laser frequencies as the measurement images.

Other past efforts to avoid this geometric scattering include changing the color of the background scattered light by treating the surface with a fluorescent coating that absorbs the laser light and re-emits it at a different wavelength. This re-emitted light can then be blocked out by an optical filter, as described by Cadel et al. (2016). Other past efforts, specific to PIV, include post-processing algorithms that remove background contributions, such as those described by Mejia-Alvarez and Christensen (2013) and Honkanen and Nobach (2015) and coloring the flow tracer particles with a fluorescent dye to use fluorescent emissions at wavelengths different from the incident laser light wavelength [Petroskey et al. (2015) and Danehy et al. (2012)].

Providing an alternative method to those mentioned above, we discuss a means for reducing, or even eliminating, the effects of background scattering with the application of structured laser illumination planar imaging (SLIPI) [e.g., see Neil et al. 1997] which is presented for the first time, to the authors' knowledge, for removing background in Doppler-based velocity measurements. This method is demonstrated in a simulated, in situ measurement environment where the exhaust of a turbulent jet located near a curved wall boundary is measured using CC-DGV. The results indicate that velocity bias errors arising from background scattering are reduced to levels expected for pristine measurement situations in which background contributions are negligible.

2 Cross-Correlation Doppler Global Velocimetry

In past works CC-DGV has been presented as a simple and robust technique for measuring three-component velocities, and has been demonstrated to provide high spatial resolution measurements, with low uncertainty values of ± 2 m/s (absolute) over a nearly unlimited dynamic range [Cadel et al. (2015), Cadel et al. (2016), Fischer et al. (2008)]. The basic working principle behind CC-DGV, as seen in Figure 1, is that a single-frequency laser beam is split into two paths, a low-power reference path and a high-power measurement path [Figure 1(a)]. Two photodetectors in the reference path are used to measure the transmission of the reference beam passing through a reference molecular vapor cell, which is a function of the wavelength of the laser emission. The beam used for flow measurements is formed into a sheet and directed through the flow interrogation region. Laser light is then scattered off small tracer particles in the flow (i.e., flow seeding), through elastic Mie scattering. This scattered light, now carrying flow velocity information in the form of a Doppler frequency shift, is collected using a camera immediately after passing through a molecular vapor cell identical to the one present in the reference path. In our applications, iodine vapor is used in the optical cells, which has been well characterized by Forkey et. al (1997) for wavelengths near 532 nm and allows us to resolve the imaged light in frequency space.

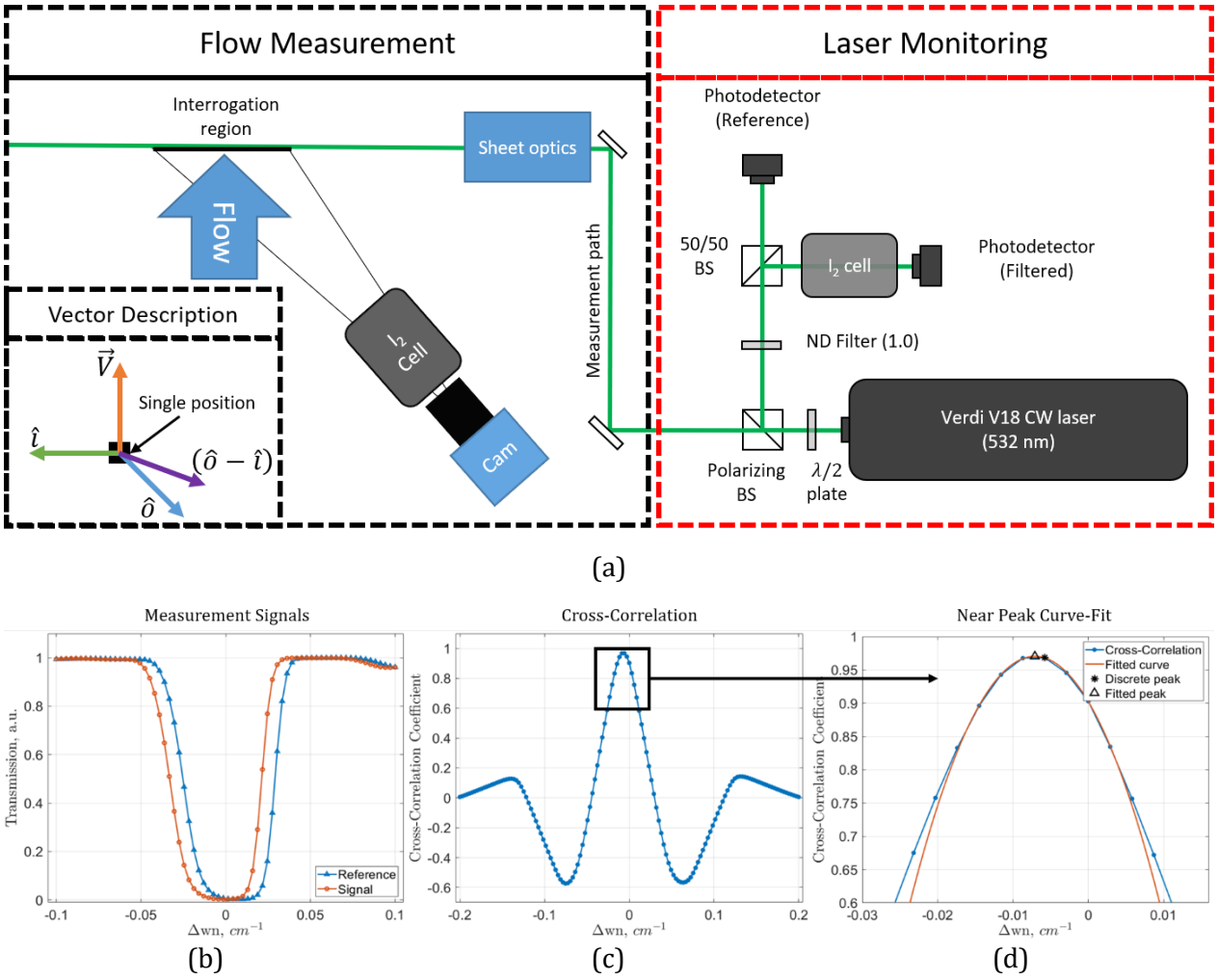

Figure 1. Cross-correlation DGV hardware and processing. This figure shows the laser frequency monitoring and basic measuring arrangement for a single camera (a) with an inset in the lower left giving a basic measurement vector $(\hat{o} - \hat{\imath})$ description. Parts (b), (c), and (d) are produced to mirror Cadel et al. 2015 Fig. 3 and show a graphical description of the steps taken in CC-DGV processing.

Measurement spectra are recorded simultaneously from both the reference path and the interrogation region by recording the transmission value through the vapor cell at a discrete set of laser light frequencies, as seen in Figure 1(b), which includes at least one absorption line associated with characteristics of the vapor in the cell. Cross-correlating the reference and flow spectra yields the cross-correlation coefficient as a function of the frequency shift between them (Figure 1(c)). The cross-correlation spectrum is then parabolically curve-fit near the maximum value to obtain an analytical lineshape in this region. The frequency shift associated with the maximum value of this parabola is then taken as the average local Doppler frequency shift [Cadel et al. 2015], which can then be related to flow velocity. The final vector velocity measurement from CC-DGV is obtained in the same way as other Doppler-based methods, using the Doppler equation,

$$\Delta\nu = \frac{(\hat{o} - \hat{\imath}) \cdot \vec{V}}{\lambda} \tag{1}$$

where $\Delta\nu$ is the measured Doppler frequency shift as a result of the local flow velocity, $\vec{V}$, the wavelength of the incident light, λ, and the optical geometry parameters, $\hat{o}$ and $\hat{\imath}$ which are the local scattered light unit vector direction for the camera position and the laser direction unit vector at a single pixel, respectively. To obtain three-component velocity at a single point, one must measure the Doppler shift in three independent arrangements of $(\hat{o} - \hat{\imath})$ [see Charrett et al. (2007) for an analysis

of errors associated with obtaining multi-view measurements]. For this application, the flow was observed from three different detector positions simultaneously, providing the required variation of $(\hat{o} - \hat{\imath})$. The three measured Doppler shift velocities are then rotated into orthogonal components by

$$\begin{bmatrix} U \\ V \\ W \end{bmatrix} = \begin{bmatrix} (\hat{o}-\hat{\imath})_{1x} & (\hat{o}-\hat{\imath})_{1y} & (\hat{o}-\hat{\imath})_{1z} \\ (\hat{o}-\hat{\imath})_{2x} & (\hat{o}-\hat{\imath})_{2y} & (\hat{o}-\hat{\imath})_{2z} \\ (\hat{o}-\hat{\imath})_{3x} & (\hat{o}-\hat{\imath})_{3y} & (\hat{o}-\hat{\imath})_{3z} \end{bmatrix}^{-1} \begin{bmatrix} U_1 \\ U_2 \\ U_3 \end{bmatrix} \tag{2}$$

where the subscripts of $(\hat{o} - \hat{\imath})_{n\xi}$ represent the ξ-component of $(\hat{o} - \hat{\imath})$ for the n^{th} detector, U_n is the measured Doppler velocity from the n^{th} detector [i.e., $(\hat{o} - \hat{\imath}) \cdot \vec{V} = \lambda \Delta \nu$ in Equation (1)], and U, V, and W are the flow velocities expressed in Cartesian coordinates [Cadel et al. (2015)].

3 Structured Laser Illumination Planar Imaging

The SLIPI method is the result of combining two separate imaging techniques, structured light and laser light sheet imaging. The structured light technique was developed by Neil et al. (1997) to improve three-dimensional imaging using a conventional wide-field microscope, while laser sheet imaging has been common practice in laser diagnostics for many years. The SLIPI method was developed, and has primarily been used, to suppress multiply-scattered light in sprayed particle visualization experiments [Kristensson et al. (2014)]. Kristensson et al. (2014) determined that the multiply-scattered light removed in the sprayed particle experiments is identical to stray/background scattering in terms of some key characteristics and was able to successfully evaluate how well the SLIPI method was able to remove stray light in determining the temperature of a CH_4/air flame with varying background complexity using Rayleigh thermometry. The method has also been applied to quantitative imaging of thermographic phosphor particles for gas phase temperature measurements [Zentgraf et al. (2017) and Stephan et al. (2019)], underscoring the versatility of the approach.

SLIPI background removal relies upon the intensity modulation of an illumination laser sheet with a uniform and well-defined spatial frequency. The Mie-scattered photons originating directly from this pattern retain the imposed pattern, and any light that is scattered from other sources show up as inconsistencies. Because these occurrences can be differentiated from the pattern applied to the laser sheet, they can be evaluated for and removed.

The most common way to remove the unwanted stray light in a specific region of interest is to record a series of images at different phase shifts from the original pattern position. For example, the intensity pattern phase shifts for a SLIPI implementation using three images would be $\phi_1 = 0^o, \phi_2 = 120^o$, and $\phi_3 = 240^o$. The corrected signal image with the stray light removed is then calculated from the series of images given by Kristensson et al. (2014) as:

$$I_S = \sqrt{\left(I_{\phi_1} - I_{\phi_2}\right)^2 + \left(I_{\phi_1} - I_{\phi_3}\right)^2 + \left(I_{\phi_2} - I_{\phi_3}\right)^2} \tag{3}$$

and adapted from a three-image series into a general number of phase shifts as:

$$I_s = \left[\sum_{\substack{i,j=1 \\ i \neq j}}^{N} \left(I_{\phi_i} - I_{\phi_j}\right)^2 \right]^{1/2} \tag{4}$$

where I_S is the composite laser sheet image, I_{ϕ_x} is the recorded sinusoidal light sheet image of the x^{th} phase shift, and N is the total number of recorded phase shifts. This method removes the intensity that is present in all the phase-shifted images at every pixel, and the remaining differences are dominated by the modulated intensity pattern. An example of three-image SLIPI background removal from the current work can be seen in Figure 2.

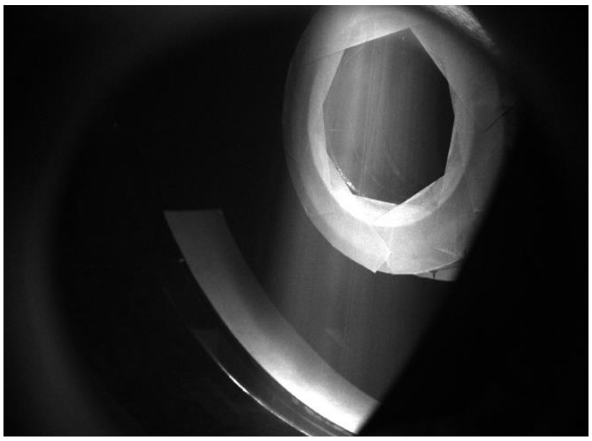

(a) Conventional DGV

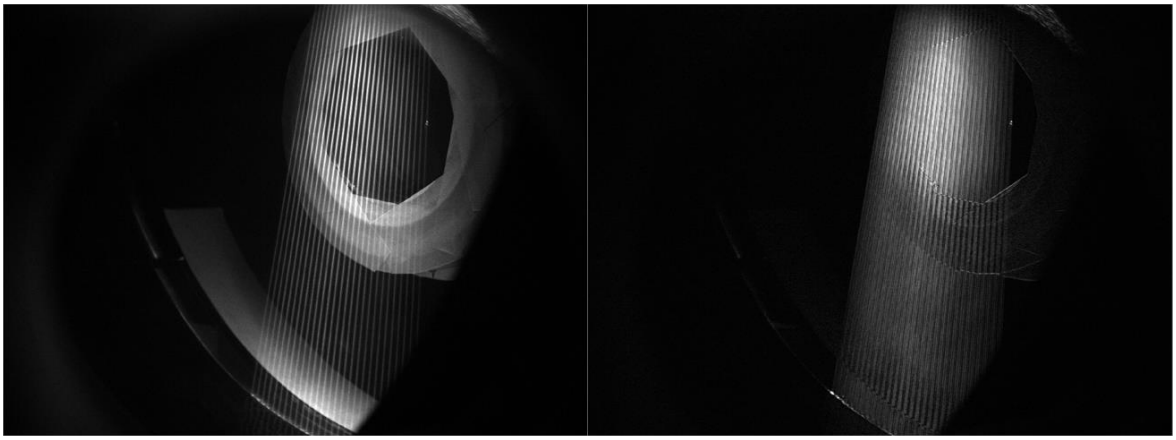

(b) Single SLIPI image (c) Processed SLIPI image

Figure 2: Background intensity comparison between conventional planar sheet image (a) and images collected using the SLIPI method (b) and (c). (b) is provided to show the intensity of the SLIPI images prior to the application of the SLIPI processing method.

Although the SLIPI method is extremely effective at removing the stray light scattering from an image, there is one main limitation associated with it. Since the camera is only able to measure a limited dynamic range of intensities, the maximum intensity (signal + background) that background can be effectively removed is then limited to the saturation intensity of the camera. By simple inspection of equation 3, we can see that if a region of the image is saturated in all individual SLIPI images, the intensity of the resultant image in that region will be zero, and no measurement signal is extracted. Therefore, the total intensity recorded must be below the saturation threshold of the camera to be able to extract any measurement information.

The main disadvantage of this technique applies directly to the chosen application of multi-image SLIPI background removal. This method requires that a minimum of three images to be taken to obtain a single measurement point with the background removed. This effectively triples the acquisition time of the measurement, but since CC-DGV is a mean velocity measurement in any case, it is presented as a validation of this technique for velocity measurements. The approach results in a modest increase in optical complexity when compared to conventional DGV measurement, while dramatically reducing stray and background light contributions. (It should be noted that another, less common, post-processing technique for background removal using SLIPI is described in detail by Berrocal et al. (2012) and allows for the removal of the background intensity by the acquisition of a

single image at the expense of spatial resolution using a spatial Fourier transform technique. The reader is referred to this work as well as [Kristensson et al. (2014)] for further details.)

4 Experiment Description

The flow apparatus and CC-DGV setup are depicted in Figure 3, consisting of a blower-driven jet flow, a duct and the optical components of the CC-DGV system. The primary objective in the current setup was to demonstrate the effectiveness of the SLIPI technique for planar mean velocity measurements in a confined environment with complex scattering and limited optical access.

The flow was driven by a Busch Panther WA13125DP rotary lobe, positive displacement blower capable of discharging 1571 CFM at the ambient conditions of 14.7 psia and 70^{o}F with an outlet diameter of 6 inches. The flow was directed, using a double bend, to the measurement region using PVC ducting, contracted down to an exit diameter of 3 inches, and exhausted into the test section at ambient pressure 1 inch upstream of the measurement location, creating a turbulent jet flow with an approximate exit Mach number of 0.5. This flow was characterized by traversing a Kiel-type probe, measuring total pressure and total temperature, across the centerline of the nozzle exhaust in increments of 0.125 inches. To simulate some aspects of the confinement for in situ measurement application, the measurement region was positioned inside of a round 21 inch diameter duct, analogous to the walls of a round wind tunnel. The laser sheet entered and exited the duct through two anti-reflection-coated acrylic windows above and below the flow, respectively.

Three camera assemblies were used to image the flow region. These assemblies were all located downstream of the nozzle and were arranged such that there was one assembly each to image from the port and starboard sides of the duct. The third assembly was positioned above the duct. Basic schematics of the described camera arrangement and flow region are also included in Figure 3, while a description of the imaging modules used can be found in section 4.2. The challenge incurred from high background interference was intentionally increased in this study by adding a layer of light-colored masking tape to both the nozzle and the duct wall to scatter more background light into the measurement. This treatment can be seen in the conventional planar image and the single SLIPI image in Figures 2(a) and (b), respectively. The laser power and exposure times were adjusted to avoid camera saturation.

4.1 SLIPI Implementation

Past applications of SLIPI have often utilized a Ronchi grating to create the intensity modulation in the laser light sheet, but due to the low damage tolerance of these types of gratings, along with the high laser powers required in imaging large fields of view in DGV, an alternative method had to be devised to impose the pattern. Kristensson et al. (2014) and Kempema et al. (2014) found that, in order to accommodate the laser energy required for Rayleigh scattering thermometry, they could induce optical interference patterns in their laser sheets by the implementation of a two-faceted optical component and by a split-beam method, respectively. In our application, we chose to create a custom subtractive grating by machining an aluminum blank with equally-spaced slots for a physical line pair width of 0.030”. This provided further optical simplicity with the added benefit of adjustability for the imaged pattern size by changing the relative positions of the grating and the sheet-forming cylindrical lens. As a subtractive grating, a major drawback is the loss of about 50% of the total laser light originally present in the beam. The arrangement used in this study can be seen in the lower right of figure 3, where the SLIPI grating is placed after the f = -9.7 mm cylindrical lens and the mirror used to direct the sheet into the duct. It should be noted that in this implementation the high intensity sections of the sheet modulation were thinner than the low intensity sections, resulting in combined images with low intensity streaks as seen previously in Figure 2. This had the effect of slightly worsening our resolvable spatial resolution.

4.2 CC-DGV Instrument

The CC-DGV instrument setup consists of a continuous wave laser, laser reference monitoring, flow illumination optics, and camera modules, and is depicted in Figure 3.

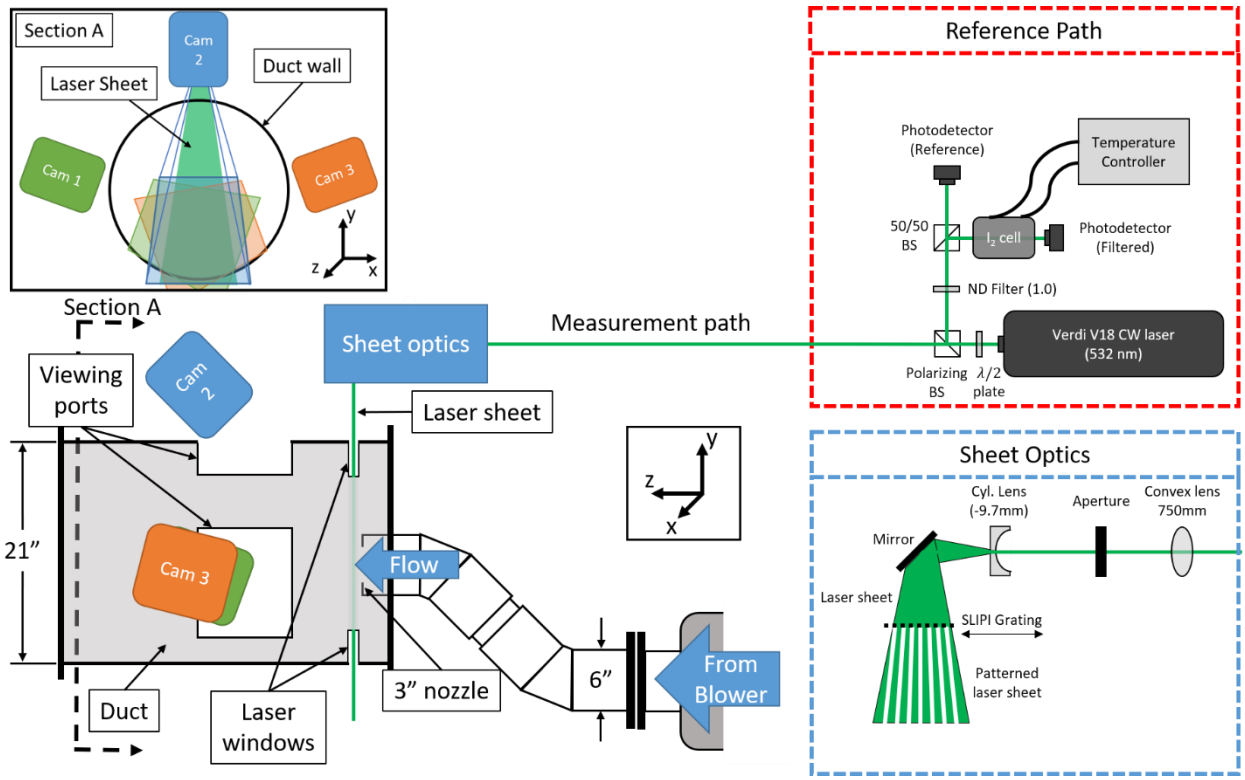

Figure 3. Experimental setup used in DGV experiments. This figure shows the experimental and optical arrangements used to collect the data used in the present work. The sector titled “Reference Path” in the upper right shows the laser frequency monitoring arrangement. The sector titled “Sheet Optics” in the lower right of shows a basic schematic of the sheet forming optics and SLIPI Grating positioning. The imaging arrangement used is detailed in the upper left and the viewing configuration described by Section A. The shaded regions inside of the duct represent the approximate field of view of the cameras

A continuous wave Coherent Inc. Verdi V18 model laser is used. This laser is a single frequency, diode-pumped, solid-state laser with a maximum output power of 18 W at 532 nm and a linewidth of 5 MHz. The emitted beam has a diameter of 2.25 mm with a beam divergence of less than 0.5 mrad. The laser frequency may be coarsely adjusted, on the order of tens of gigahertz, via the internal etalon, while finer-scale frequency tuning may be achieved by changing the internal cavity length in the laser head using a piezoelectric stack (PZT). The bandwidth of the fine-tuning range of the PZT is about 6.4 GHz. The frequency scanning required for the CC-DGV measurements is done by applying a voltage to the PZT using a BK Precision DC power supply with a voltage range of 0 to 72 V. Frequency monitoring of the laser is done by collecting the transmission spectrum through a molecular vapor cell containing iodine. The iodine cell used is an ISSI I2S-5, which is 5 inches long and 3 inches in diameter and is operated in a starved cell configuration with a vapor pressure of 0.675 Torr and a body temperature of 65^{o}C. This configuration is used to prevent fluctuations in vapor pressure with cell temperature during testing by operating at least 20^{o}C above the point where all the iodine in the cell will exist in the vapor state. To collect the reference transmission spectrum, the reference path (upper right of Figure 3) is split into two paths using a 50/50 beam splitter, and the intensity of each path is monitored using a ThorLabs PDA100A Si free-space amplified photodetector (PD). One of the paths travels directly to a PD and is used normalize laser output power fluctuations, while the second PD is

used to measure the intensity of the beam passing through the reference iodine cell. The ratio between the two reference PD signals provides the reference iodine transmission spectrum. A theoretical spectral model for iodine absorption developed by Forkey et al. (1997) is then used to map the applied PZT voltage to frequency relative to the center of the chosen iodine absorption line.

To expand the measurement path beam into a laser sheet and impose the intensity pattern on it, the beam is directed to the sheet forming optics, expanded using a -9.7mm focal length cylindrical lens and then passed through the custom grating to form the patterned laser sheet, seen in the lower right of Figure 3. This sheet is then passed through the test section and imaged using three different camera module assemblies, seen in the section view of the imaging environment in the upper left of Figure 3.

The camera modules consist of two FLIR, 12 bit, Blackfly S model BFS-U3-31S4M-C, machine vision cameras, both with identical 16mm c-mount lenses and 532nm band pass filters, in addition to an ISSI I2S-5 iodine molecular vapor filter identical to the one used in the reference laser beam frequency monitoring setup. The vapor cell was mounted in front of a single camera to record the filtered images, while the other camera was positioned to record images view the same interrogation region and serve as the intensity reference for the filtered camera.

5 Results

The results presented in this work are used to demonstrate the capability of SLIPI background removal in Doppler-based velocity measurements, specifically its effectiveness in eliminating background/geometrical scattering contributions in cross-correlation Doppler global velocimetry which lead to biases in measured velocities. Kiel-probe total pressure and temperature measurements were taken at the horizontal centerline of the nozzle, near the axial plane where the CC-DGV measurements to serve as a velocity reference. This reference and the CC-DGV measurements were then directly compared to provide a quantitative error analysis for the DGV measurements. In addition to the probed exit velocity, the total conditions in the plenum were also monitored using a Pitot-static total pressure probe and a K-type thermocouple for all test cases. With the ambient pressure of the room known, one may readily calculate the isentropic exit velocity, assumed as representative along the centerline of the jet.

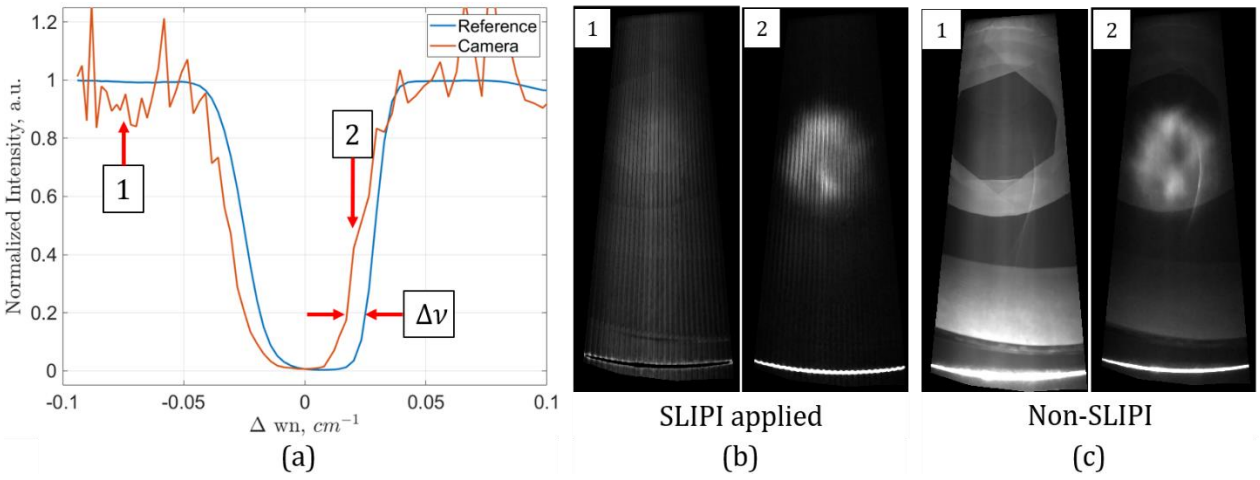

Figure 4. Example measurement spectrum corresponding to a position inside of the potential core of the jet (a) and two sample images taken from camera 2 in both SLIPI background removal (b) and conventional laser sheet imaging (c).

Three sample images collected at different laser frequencies in the scan are provided in Figure 4 to show the effect of the Doppler shift, as well as the difference in background between the SLIPI and conventional sheet image collection. Figure 4(b) shows the effectiveness of the SLIPI method in removing the unwanted background scattering clearly seen in Figure 4(c) at both positions in the

transmission spectrum. We also see that the outlined limitation concerning camera saturation is present in the bottom of Figure 4(b), where the laser directly impacts the window. A surprising result from this basic analysis is that SLIPI was very effective at removing the reflected laser light from the lower window, seen as a bright streak near the center of both images in Figure 4(c). The reflection was seen in the individual SLIPI images but automatically removed, as if it were background, by application of equation (3).

5.1 Three-Component Velocity Results

The raw or camera sensed and three-component velocity contours of this flow region for the SLIPI-CCDGV application can be found in Figure 5(a) and (b), respectively. The application of SLIPI to the CC-DGV technique has allowed the recovery of interesting structure in the secondary flow that is realistic given (1) the double-bend in the 6" plenum and (2) setup-specific entrainment that was observed in the lower portion of the rig [the positive V velocity present for Y<-50 mm in Figure 5(b)].

The raw, camera sensed velocities from the SLIPI processing (Figure 5(a)) are all similar in shape and extent, while variations across the plume appear to be sufficiently resolved to indicate true secondary flow velocities arising from the experimental setup. We can also note the smooth contour seen in the W-velocity plot indicative of the nearly constant velocity core of the jet to the gradient outside of the core representing the developing shear layer as a result of this experimental setup.

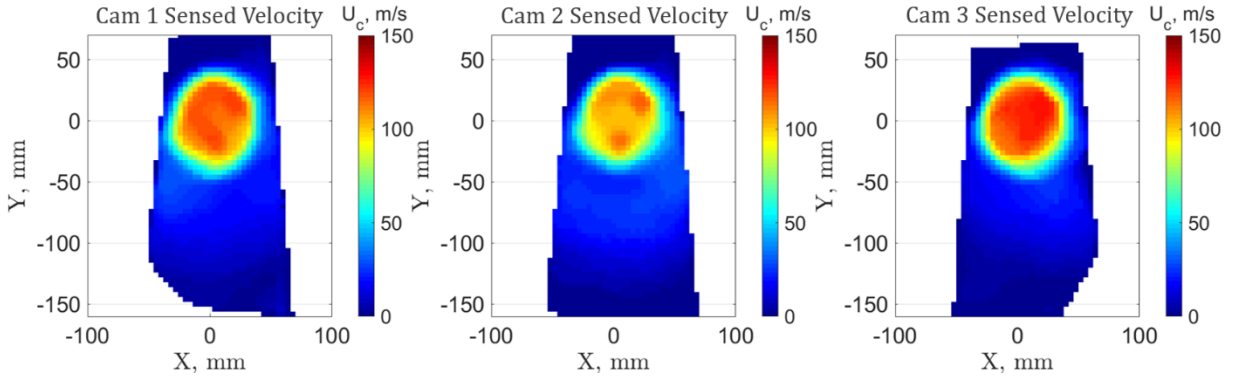

(a)

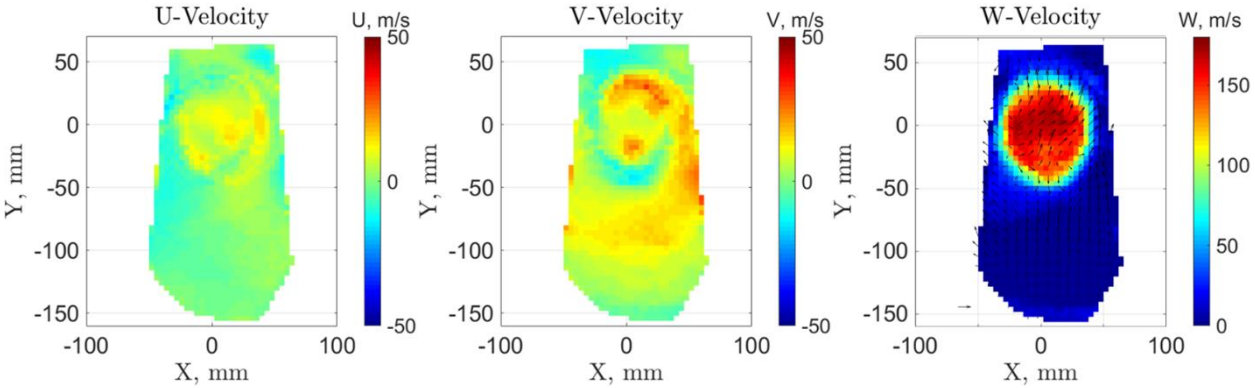

(b)

Figure 5. Raw, camera sensed (a) and Orthogonal (b) velocity contours from CC-DGV with SLIPI background removal applied. The W-velocity contour in (b) also includes an overlay of the in-plane velocities with a reference vector located in the lower left indicating a velocity of 20 m/s.

Quantitative comparisons to flow reference measurements obtained using a Kiel probe allow a more rigorous assessment of the velocity results obtained using CC-DGV. With the ambient conditions known, the total velocity of the flow was calculated via first law of thermodynamics and isentropic relations using,

$$V_{tot} = \sqrt{\frac{2\gamma RT}{\gamma - 1}\left[\left(\frac{p_0}{p}\right)^{\frac{\gamma-1}{\gamma}} - 1\right]} \tag{5}$$

where p_0 is the measured total pressure, p is the ambient static pressure, and T is the static temperature of the flow. For velocity comparisons, we calculate the total velocity of the CC-DGV measurements from all three orthogonal components of velocity measured as,

$$V_{tot} = \sqrt{U^2 + V^2 + W^2} \tag{6}$$

Figure 6(a) shows the location of the probe-measured profile on the total velocity contour, and as such, the position where the comparison data were taken. Figure 6(b) shows the probe-derived and DGV-derived total velocity profiles, located at the horizontal centerline of the jet, calculated from equation (5) and (6), respectively, and plotted against one another. The velocity magnitude differences seen in the shear layer are likely due to a small difference in the axial measurement position of the CC-DGV plane with respect to the axial plane where the probe data were acquired. The SLIPI-CCDGV velocity profile closely matches the probe measurements in the core region of the jet, defined here as $-19\,mm \leq X \leq 19\,mm$, with an RMS difference of 1.2 m/s, well within the established uncertainty bounds of CC-DGV and the Pitot probe.

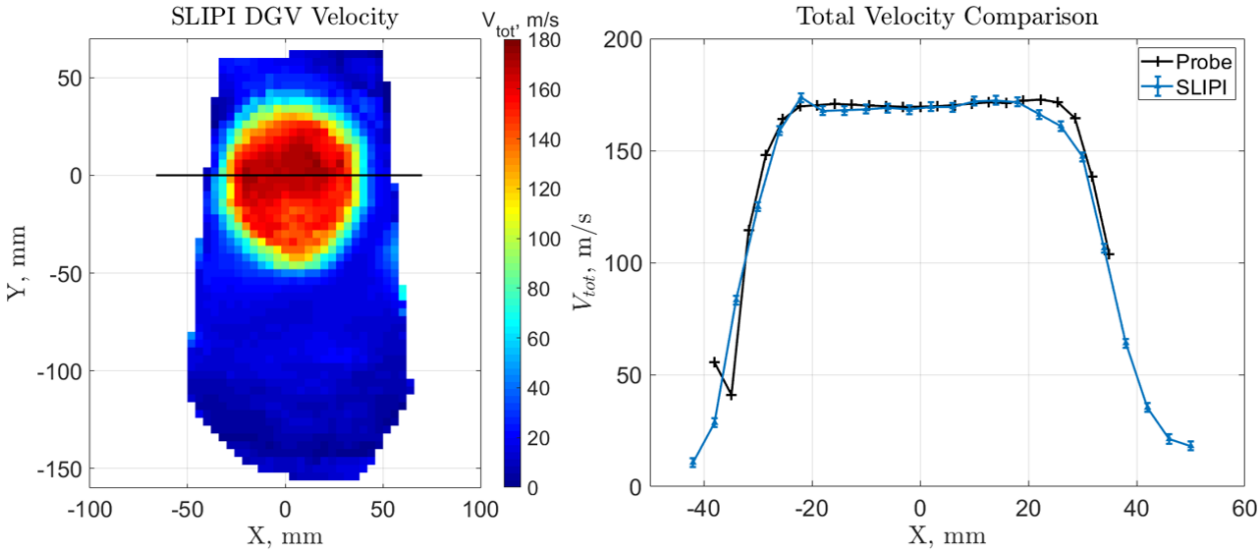

(a) (b)

Figure 6. Total velocity contour (a) and total velocity profile comparisons (b) with error bars indicating the uncertainty in the CC-DGV measurements ($\pm 2\ m/s$)

6 Conclusion

In the present work we discuss the first application of structured laser illumination planar imaging background reduction method toward eliminating the velocity measurement biases attributable to background or geometrical scattering of laser light in cross-correlation Doppler global velocimetry measurements. In this study, we interrogated the 3-component velocity profile within a 2-dimensional slice of a free jet flow located approximately 0.33 diameters downstream from the exit of a nozzle operating at a Mach number of 0.5 using the SLIPI-CCDGV method.

The results of this study show that the SLIPI method was successful in removing the intense background contributions present in this experimental setup at each of the tuned frequencies, yielding the conclusion that, with this technique, it is not required to collect background images at every frequency prior to, or after, collecting velocity data. In fact, it is presented as a method where measurement images can serve the same function as background images. Another result seen in this study is that, in addition to removing the background scattering from the recorded images, the light reflected into the measurement region by the laser exit window was also removed from the images, further proving the capability of the SLIPI method in application. Measured velocities from this method showed trends consistent with the characteristics of a free jet as well as other noted trends, such as the higher V-velocity and the non-zero secondary velocities within the core of the jet, that come as a result of the experimental flow environment. The total velocity from the SLIPI-CCDGV method was compared to Kiel-probe measurements taken at the exit of the jet, and the comparison between the two profiles showed very similar trends, with an RMS difference of 1.2 m/s in the core of the jet.

Overall, the SLIPI technique for background removal has been shown to significantly decrease the biases associated with significant background scattering in CC-DGV measurements by removing the driver for negative biases in the camera sensed velocity space altogether. The method offers a major practical benefit for in situ quantitative measurement and imaging applications in complex flow systems that often suffer from major obscuration from background light.

References

Nelson MA, Lowe KT, O'Brien WF, Kirk C, and Hoopes KM (2014) Stereoscopic PIV measurements of swirl distortion on a full-scale turbofan engine inlet, *AIAA SciTech 2014-Proceedings of 52nd AIAA Aerospace Sciences Meeting, National Harbor, MD, USA January 13-17:* paper AIAA-2014-0533

Guimarães T, Lowe KT, and O'Brien WF (2016) An overview of recent results using the StreamVane method for generating tailored swirl distortion in jet engine research, *AIAA SciTech 2016-Proceedings of 54th AIAA Aerospace Sciences Meeting, San Diego, CA, USA January 4-8,* paper AIAA-2016-0534

Guimarães T, Frohnapfel D, Lowe KT, and O'Brien WF, (2017) Complex Flow Generation and Development in a Full-Scale Turbofan Inlet, Proceedings of *ASME Turbo Expo 2017, Charlotte, NC, USA June 26-30,* paper GT2017-64756

Cadel DR and Lowe KT (2015) Cross-correlation Doppler global velocimetry (CC-DGV), *Optics and Lasers in Engineering* 71: pp51-61

Boyda M and Lowe KT (2018) Cross-Correlation Doppler Global Velocimetry using Rayleigh and Mie Scattering, *AIAA SciTech 2018-Proceedings from the 56th AIAA Aerospace Sciences Meeting, Kissimmee, Florida, USA January 8-12,* paper AIAA-2018-1766

Yeaton I, Maisto P, and Lowe KT (2012) Time resolved filtered Rayleigh scattering for temperature and density measurements, *Proceedings from the 28th AIAA Aerodynamic Measurement Technology, Ground Testing, and Flight Testing Conference, New Orleans, LA, USA June 25-28,* paper AIAA-2012-3200

Boyda, MT, Byun, GB, and Lowe K.T, (2019) Investigation of velocity and temperature measurement sensitivities in cross-correlation filtered Rayleigh scattering (CCFRS), *Measurement Science and Technology* 30:044004

Doll U, Stockhausen G, Willert C (2014) Endoscopic filtered Rayleigh scattering for the analysis of ducted gas flows, *Experiments in Fluids* 55:1690

Doll U, Dues M, Tommaso B, Picchi A, Stockhausen G, Willert C (2018) Aero-thermal flow characterization downstream of an NVG cascade by five-hole probe and filtered Rayleigh scattering measurements, *Experiments in Fluids* 59:150

Treaster, AL, and Yocum, AM, (1978) "The Calibration and Application of Five-Hole Probes," *Proceedings from the 24th International Instrumentation Symposium, No. TM 78-10*, *Albuquerque, New Mexico, USA January 18*

Mejia-Alvarez R and Christensen KT (2013) Robust suppression of background reflections in PIV images, *Measurement Science and Technology* 24:027003

Honkanen M, Nobach H (2015) Background extraction from double-frame PIV images, *Experiments in Fluids* 38: pp348-362

Cadel DR, Shin D, and Lowe KT (2016) A hybrid technique for laser flare reduction. *AIAA SciTech 2016-Proceedings from the 54th AIAA Aerospace Sciences Meeting, San Diego, California, USA January 4-8,* paper AIAA-2016-0788

Petroskey JP, Maisto P, Lowe KT, André MA, Bardet PM, Tiemsin PI, Wohl CJ, and Danehy PM (2015) Particle image velocimetry applications using fluorescent dye-doped particles. *AIAA SciTech 2015-Proceedings from the 53rd AIAA Aerospace Sciences Meeting, Kissimmee, FL, USA January 5-9,* paper AIAA-2015-1223

Danehy PM , Tiemsin PI, Wohl CJ, Verkamp M, Lowe KT, Maisto P, Byun G, and Simpson R (2012), Fluorescence-doped particles for simultaneous temperature and velocity, *NASA Technical Memorandum,* NASA TM-2012-217768

Cadel DR and Lowe KT (2016) Investigation of measurement sensitivities in cross-correlation Doppler global velocimetry, *Optics and Lasers in Engineering* 86: pp 44-55

Fischer A, Büttner L, Czarske J, Eggert M, Müller H (2008) Measurement uncertainty and temporal resolution of Doppler global velocimetry using laser frequency modulation, *Applied Optics* 47:21: pp3941–3953.

Forkey JN, Lempert WR, and Miles RB (1997) Corrected and calibrated I2 absorption model at frequency-doubled Nd:YAG laser wavelengths, *Applied Optics* 36:27: pp6729-6738

Charrett TOH, Nobes DS, and Tatam RP (2007) Investigation into the selection of viewing configurations for three-component planar Doppler velocimetry measurements. *Applied Optics* 46:19: pp4102-4116

Neil MAA, Juškaitis R, and Wilson T (1997) Method of obtaining sectioning by using structured light in a conventional microscope. *Optics Letters* 22:24: pp1905-1907

Kristensson E, Ehn A, Bood J, and Aldén M (2014) Advancements in Rayleigh scattering thermometry by means of structured illumination, *Proceedings of the Combustion Institute* 35: pp3689-3696

Zentgraf, F., Stephan, M., Berrocal, E., Albert, B., Böhm, B. and Dreizler, A., 2017. Application of structured illumination to gas phase thermometry using thermographic phosphor particles: a study for averaged imaging. *Experiments in Fluids* 58:82

Stephan, M., Zentgraf, F., Berrocal, E., Albert, B., Böhm, B. and Dreizler, A., 2019. Multiple scattering reduction in instantaneous gas phase phosphor thermometry: applications with dispersed seeding. *Measurement Science and Technology,* 30:054003

Berrocal E, Johnsson J, Kristensson E, and Aldén M (2012) Single scattering detection in turbin media using single-phase structured illumination filtering, *Journal of the European Optical Society-Rapid Publications* 7:12015

Kempema NJ and Long MB (2014) Quantitative Rayleigh thermometry for high background scattering applications with structured laser illumination planar imaging, *Applied Optics* 53:29: pp6688-6697